Caveolin-1 promotes radioresistance in rhabdomyosarcoma through increased oxidative stress protection and DNA repair.

Silvia Codenotti [a,#], Francesco Marampon [b,c,#], Luca Triggiani [d], Marco Lorenzo Bonù [d], Stefano Maria Magrini [d], Paola Ceccaroli [e], Michele Guescini [e], Stefano Gastaldello [f,g], Vincenzo Tombolini [b,c], Pietro Luigi Poliani [a], Michela Asperti [a], Maura Poli [a], Eugenio Monti [a], Alessandro Fanzani [a].

Addresses

[a] Department of Molecular and Translational Medicine, University of Brescia, Brescia, Italy.

[b] Department of Pediatrics, "Sapienza" University of Rome, Rome, Italy.

[c] Department of Radiotherapy, Policlinico Umberto I, "Sapienza" University of Rome, Rome, Italy.

[d] Radiation Oncology Department, ASST Spedali Civili di Brescia, University of Brescia, Brescia, Italy.

[e] Department of Biomolecular Sciences, University of Urbino Carlo Bo, Urbino, Italy.

[f] Department of Physiology and Pharmacology, Karolinska Institutet, Stockholm, Sweden.

[g] Precision Medicine Research Center, School of Pharmacy, Binzhou Medical University, Laishan District, Guanhai Road 346, Yantai, Shandong Province, 264003 China.

[#] These authors contributed equally to this paper.

[*] Corresponding author: Alessandro Fanzani (alessandro.fanzani@unibs.it); Tel: +39-030-3717567.

Abstract

The aim of this work was to investigate whether Caveolin-1 (Cav-1), a membrane scaffolding protein widely implicated in cancer, may play a role in radioresistance of rhabdomyosarcoma (RMS), a pediatric soft tissue tumor. For this purpose, we employed human RD cells in which Cav-1 expression was stably increased by gene transfection. After irradiation, we observed that Cav-1 limited cell cycle arrest in the G2/M phase and enhanced cell survival by protection from senescence and apoptosis via reduction of $p21^{Cip1/Waf1}$, $p16^{INK4a}$ and Caspase-3 cleavage. Cav-1-mediated radioresistance was characterized by low accumulation of H2AX foci, as confirmed by Comet assay, marked neutralization of reactive oxygen species and enhanced DNA repair via activation of ATM, Ku70/80 complex and DNA-PK. Increased Cav-1 expression led to higher content of

glutathione and greater catalase expression, which protected RD cells against treatment with hydrogen peroxide. Furthermore, pre-treatment of irradiated cells with PP2 or LY294002 compounds restored radiosensitivity, indicating a role for Src-kinases and Akt pathways in Cav-1-mediated RD radioresistance. These findings were confirmed using RD and RH30 lines with acquired radioresistance obtained by hypofractionated radiotherapy, which showed marked increase of Cav-1, catalase and Akt, and sensitivity to PP2 and LY294002 treatment. In conclusion, these data suggest that Cav-1 enhances ROS protection and DNA repair through Src-kinase/Akt signaling cooperation in RMS. Furthermore, these data indicating a critical role of Cav-1 in governing catalase expression identify a vital mechanism for RMS cells to circumvent oxidative cell death.

Keywords: Caveolin-1; DNA repair; oxidative stress; radioresistance; rhabdomyosarcoma.

Introduction

Rhabdomyosarcoma (RMS) is a myogenic soft tissue tumor that represents about 4.5% of all childhood cancer cases. It is subdivided into two main groups, termed embryonal (ERMS) and alveolar (ARMS), which show distinct tumor location, histology, genetic signatures, and outcomes [1]. ERMS represents about 70% of all RMS cases and typically affects children less than 10 years. ARMS, affecting adolescents, is more aggressive because of a chromosomal translocation leading to the fusion of paired box 3 (PAX3) gene (in a minority of cases the PAX7 gene) and the forkhead box O1 (FOXO1) gene, which generates a chimeric transcription factor with pro-metastatic activity [2]. To improve local control and outcome, RMS treatment involves a combined approach, based on radiotherapy and chemotherapy. However, these treatments may give rise to resistance mechanisms that lead to relapse and treatment failure [3]. Thus, identification of the molecular mechanisms underpinning radio- and chemoresistance is a challenge to overcome aggressive tumors. Caveolin-1 (Cav-1) is the major protein component of caveolae, cholesterol-enriched lipid rafts of the plasma membrane implicated in several processes, including endocytosis, mechano-protection and regulation of signal transduction [4, 5]. In cancer, it is widely accepted that loss of Cav-1 correlates with early-stage tumor progression [6, 7], while its re-expression and phosphorylation is associated with recurrence and metastatic disease [8, 9]. Cav-1, being involved in the regulation of cell signaling [10], oxidative stress response [11] and DNA repair [12], has been associated with

chemo- and radioresistance in several tumors [13, 14], including pancreatic cancer [15], lung cancer [16], breast cancer [17], lymphoblastoid cancer cells [18], squamous carcinoma cell line [19], colorectal cancer [20] and gliomas [21]. Over the last 10 years, we and others have shown that Cav-1 cooperates to tumor growth and metastatic potential in ERMS [22-27]. In the present work, we show that increased Cav-1 expression in human RD cells enhances both protection against oxidative stress and DNA repair, therefore promoting radioresistance.

Materials and Methods

Reagents and antibodies were from Sigma-Aldrich (Milan, Italy) and Santa Cruz Biotechnology (Dallas, TX, USA), respectively, unless otherwise stated.

Antibodies.

Primary antibodies were: anti-total and -phosphorylated Cav-1 (Tyr14) (code sc-894; code 611338, BD Biosciences, Buccinasco, Italy), anti-total and -phosphorylated checkpoint kinase 1 (Chk1) (Ser345) (code sc-8408; code 2348, Cell Signaling Technology, Danvers, MA, USA), anti-total and -phosphorylated checkpoint kinase 2 (Chk2) (Thr68) (code sc-5278; code 2197, Cell Signaling Technology, Danvers, MA, USA), anti-Caspase-3 (code NB100-56113, Novus Biological Europe, Abingdon, UK), anti-$p21^{Cip1/Waf1}$ (code sc-6246), anti-$p16^{INK4a}$ (code sc-1207), anti-total and -phosphorylated histone H2AX (Ser139) (code sc-517336; code 9718, Cell Signaling Technology, Danvers, MA, USA), anti-total and -phosphorylated ataxia telangiectasia mutated (ATM) (Ser1981) (code sc-377293; code sc-47739), anti-Ku70 (code sc-17789), anti-Ku80 (code sc-5280), anti-total and -phosphorylated DNA-dependent protein kinase (DNA-PK) (phospho S2056) (code sc-390698; code ab18192, Abcam, Cambridge, UK), anti-Catalase (H9) (code sc-271803), anti-total and -phosphorylated Ak strain transforming murine thymoma viral oncogene (Akt) (Ser473) (code sc-8312; code sc-7985), anti-beta-Tubulin (code MA5-16308, Thermo Scientific, Rockford, USA). The secondary antibodies were anti-mouse (code sc-516102) and anti-rabbit (code sc-2357).

Beta-galactosidase assay.

Cell senescence was evaluated by using a specific β-galactosidase assay kit (Cells Biolabs Inc., San Diego, CA, USA) on cultured living cells, according to the manufacturer's instructions.

Catalase assay.

The enzymatic activity of catalase was determined by the method of Beutler. RD^{ctrl} (1.5×10^5), $RD^{Cav\text{-}1}$ (1.2×10^5) and $RD^{Cav\text{-}1/F2}$ (1.2×10^5) cells were plated in 6-well plates. After 48 hours, cells were washed twice with phosphate buffer solution (PBS) and scraped in 5 mM KH_2PO_4/Na_2HPO_4 buffer (containing 3 mM KF and 3 mM β-Mercaptoethanol, pH 7.5). The obtained suspension was sonicated three times with 10 seconds pulse and then centrifuged at 12,000×g for 10 minutes (4°C). Ethanol was added to the supernatant to stabilize the lysate by breaking down 'complex II' of catalase and hydrogen peroxide (H_2O_2). After the addition of 50 µl of 1M Tris-HCl, 5mM EDTA (pH 8.0), 450 µl of H_2O_2 and 450 µl of H_2O to the cuvettes, the reaction was incubated for 10 minutes (37°C); then sample is added, and catalase activity was measured spectrophotometrically by monitoring the decrease in absorbance at 230 nm wavelength caused by the disappearance of H_2O_2. One unit of catalase activity is defined as 1 µmol of H_2O_2 decomposed per minute under the assay conditions (ε230=0.071). Catalase activity was expressed as U/mg of proteins.

Cell culture.

Human RD and RH30 cell lines were purchased from the European Collection of Cell Cultures (ECACC, Salisbury, UK). RD cells engineered for Cav-1 overexpression ($RD^{Cav\text{-}1}$) and lung metastasis derived $RD^{Cav\text{-}1/F1}$ and $RD^{Cav\text{-}1/F2}$ lines were obtained as previously described [23, 26]. All cell lines were routinely maintained in a humidified incubator at 37°C, 5% CO_2 in high-glucose Dulbecco's Modified Eagle's Medium (DMEM) supplemented with 10% fetal bovine serum (FBS) (Life Technologies, Monza, Italy), 100 mg/ml penicillin/streptomycin antibiotics and 1 mM L-glutamine. Stably transfected cells were maintained in G418 antibiotic-supplemented growth medium.

Clonogenic assay.

Post-irradiated cells were trypsinized and plated into 6-well plates in triplicate (at a density of 500 cells/well) to evaluate clonogenic survival. After 11 days, colonies were fixed with 3% paraformaldehyde (PFA)/PBS solution for 20 minutes (4°C) and stained with 0.2% crystal violet/PBS solution (with 20% methanol) for 10 minutes at room temperature (RT). Wells were washed with deionized water and pictures of colonies were taken. Then, the dye was solubilized in 1% sodium dodecyl sulfate (SDS)/PBS solution. Plates were shaken until complete dissolution was achieved, and then absorbance was measured by reading the plate at 595 nm emission wavelength.

Comet assay.

The neutral comet assay was performed by using the Comet Assay Kit (Abcam, Cambridge, UK), according to the manufacturer's instructions. Images were acquired by a fluorescent Axiovert microscope (Carl Zeiss, Oberkochen, Germany) using the ImagePro Plus software (Media Cybernetics Inc., Rockville, MD, USA). The percentage of tail DNA was calculated using OpenComet plugin from ImageJ software.

Drug inhibitor and irradiation treatments.

The PP2 and LY294002 compounds, two potent inhibitors of several Src-kinase and Phosphatidylinositol-4,5-bisphosphate 3-kinase (PI3K) family members, respectively, were dissolved in dimethyl sulfoxide (DMSO) vehicle. Irradiation (IR) treatment was performed at RT on 80% confluent cells at different Gray (Gy) doses using an X-ray linear accelerator (dose rate of 2 Gy/minute).

FACS analysis.

Post-irradiated cells were harvested after 24 hours and pellets were fixed in 0.5% PFA/PBS solution for 1 hour (4°C). Then, samples were washed with PBS twice and suspended in PBS with 50% fetal calf serum (FCS) and 70% ethanol. Cells were left at 4°C, avoiding light exposure, until FACS analysis was performed using Coulter Epics XL Flow Cytometer (Beckman Coulter, Brea, CA, USA).

Glutathione assay.

To determine the cellular content of reduced glutathione (GSH), RD^{ctrl} (1.5×10^5), $RD^{Cav\text{-}1}$ (1.2×10^5) and $RD^{Cav\text{-}1/F2}$ (1.2×10^5) were plated in 6-well plates. After 48 hours, cells were washed twice with PBS, detached by scraping with a rubber policeman and immediately lysed with 100 µl of lysis buffer (0.1% Triton X-100, 0.1 M Na_2HPO_4, 5 mM EDTA, pH 7.5). Thereafter, 15 µl of 0.1 M HCl and 140 µl of precipitating solution (100 ml containing 1.67 g of glacial metaphosphoric acid, 0.2 g of disodium EDTA and 30 g of NaCl) were added. After recovery, samples were kept on ice for 10 minutes and then centrifuged at 12,000×g for 10 minutes (4°C). Six hundred µl of 0.3 M Na_2HPO_4 were added to 200 µl of the acid extract (Blank) and then 80 µl of 1% 5,5-dithio-bis-2-nitrobenzoic acid (DTNB) solution/sodium citrate solution. GSH determination was measured spectrophotometrically at 412 nm wavelength ($\varepsilon412=13600\ M^{-1}\ cm^{-1}$). Pellet protein content was assayed by Bradford's method.

Immunoblotting.

Sample preparation was made as previously described [26]. Band densitometry was calculated using the Gel Pro Analyzer 4 software (MediaCybernetics Inc., Rockville, MD, USA) and expressed by arbitrary density units, setting control to 1.

Radioresistance protocol.

Radioresistant RD and RH30 lines were obtained as reported herein [28]. Briefly, parental lines were exposed to a final equivalent radiation dose of 66 Gy, fractionated in six rounds of IR delivered with a dose rate of 2 Gy/minute within a period of 33 days. Twenty-four hours after each IR round, cells were trypsinized and plated at 30% confluence before receiving the subsequent dose at 80% confluence. In our setting, radioresistance was maintained over ten passages.

Real-time PCR.

Post-irradiated cells were subjected to total RNA extraction after 24 hours by using TriPure Isolation Reagent (Euroclone, Milan, Italy), according to the manufacturer's instructions. The reverse transcription was performed by using the QuantiTect Reverse Transcription kit (Qiagen, Hilde, Germany), according to the manufacturer's instructions, for detection of nuclear factor erythroid 2-related factor (NRF2), superoxide dismutase 2 (SOD-2), catalase (CAT) and glutathione peroxidase 4 (GPx4) gene expression by real-time PCR. The cDNA miScript PCR Reverse Transcription kit (Qiagen, Hilde, Germany) was instead used, according to the manufacturer's instructions, for detection of miR-22, -34a, -126, -210 expression. Normalization was carried out using hypoxanthine phosphoribosyl transferase 1 (HPRT-1) and small nucleolar RNA, C/D box 25 (SNORD-25) as housekeeping gene and miRNA, respectively.

ROS detection.

Mitochondrial superoxide anion ($O_2 \cdot^-$) production was assessed by using the MitoSOX Red probe (Thermo Fisher Scientific, Milan, Italy) at the final concentration of 5 μM, according to the manufacturer's instructions. Data were analyzed by CellQuest software (BD Biosciences, Buccinasco, Italy) and results were represented as median of fluorescence. Total intracellular reactive oxygen species (ROS) were measured by using the OxiSelect Intracellular ROS assay kit (Cell Biolabs Inc., San Diego, CA, USA), which is based on the use of a cell-permeable fluorogenic probe 2',7'-dichlorodihydrofluorescin diacetate (DCFH-DA), according to the manufacturer's instructions. The fluorescent intensity, which is proportional to the ROS level within the cell

cytosol, was quantified by Fluoroscan Ascent FL (Thermo Fisher Scientific, Milan, Italy) at 485 nm excitation/538 nm emission wavelengths.

Statistical analysis.

Statistical significance was assessed by Unpaired Student's t-test and One-Way Anova test, using GraphPad Prism 5 software (GraphPad Software, San Diego, CA, USA). Statements of significance were based on a p-value of less than 0.05.

TUNEL assay.

Post-irradiated cells were fixed in 4% PFA/PBS solution for 20 minutes (4°C). Then, cells were stained using the TUNEL kit (Roche, Milan, Italy) to assess apoptosis, according to the manufacturer's instructions.

Results

Cav-1 promotes radioresistance in the human embryonal RD cell line.

We have previously shown that Cav-1 is expressed at low level in the human embryonal RD cells and its increased expression through stable gene transfection promotes aggressive behavior of RD cells *in vitro* and *in vivo* [23]. In order to assess whether Cav-1 may also influence radioresistance, we evaluated IR sensitivity in three RD lines carrying a higher expression of Cav-1 (total and phosphorylated form) [26], called $RD^{Cav\text{-}1}$, $RD^{Cav\text{-}1/F1}$ and $RD^{Cav\text{-}1/F2}$ (Fig. 1A). After IR, these lines formed a greater number of colonies compared to control (RD^{ctrl}), as detected by a clonogenic assay (Fig. 1B). Specifically, the IR50 Gy doses were 3.5 in RD^{ctrl}, 5 in $RD^{Cav\text{-}1}$, 5.5 in $RD^{Cav\text{-}1/F1}$ and 6.0 in $RD^{Cav\text{-}1/F2}$ (Fig. 1B), suggesting that greater Cav-1 levels correlate with radioresistance in RD cells.

Cav-1 counteracts radiotherapy-induced senescence and apoptosis.

IR-induced DNA damage activates checkpoint pathways that inhibit cell progression through the G1 and G2 phases and induce a transient delay in progression through the S phase. The cells are more radiosensitive in the G2-M phase, less sensitive in the G1 phase, and even less sensitive during the last fraction of the S phase [29]. By immunoblotting, we observed that IR induced a faster and higher phosphorylation/activation of Chk1 and Chk2 checkpoint mediators [30] in $RD^{Cav\text{-}1}$ compared to RD^{ctrl} line (Fig. 2A). As detected by flow cytometry analysis, IR treatment significantly increased the percentage of cells in the G2 phase in RD^{ctrl} line (from 7.32% to 41.37%) but not in $RD^{Cav\text{-}1}$ cells (from 8.65% to 15.52%). In addition, $RD^{Cav\text{-}1}$ cells also showed an increase

of cells in the S phase (Fig. 2B). Radiotherapy administered in fractional doses aims to increase the number of tumor cells arrested in G2/M, which will be more sensitive to the subsequent IR [31]. For this reason, we tested the effects of an additional IR treatment (4 Gy), administered 24 hours after the first one. We detected a significant increase of apoptotic and senescent cells in RD^{ctrl} compared to $RD^{Cav\text{-}1}$ line, as detected by TUNEL and β-galactosidase assays, respectively (Fig. 2C, D). Consistent with this, the cleaved Caspase-3 form and the senescence-related markers $p21^{Cip1/Waf1}$ and $p16^{INK4a}$ were increased in post-irradiated RD^{ctrl} cells compared to $RD^{Cav\text{-}1}$ (Fig. 2E, F). Overall, these data indicate that Cav-1 counteracts both IR-induced G2/M growth arrest and the mechanisms leading to cellular senescence and apoptosis.

Cav-1 protects from IR-induced DNA damage by enhanced ROS neutralization and DNA repair.

Radiotherapy produces extensive DNA damage via direct or indirect effects. Therefore, we evaluated the accumulation of histone H2AX foci, which are predictive of DNA double strand breaks (DSBs) [32]. Over a 12-hour time course, we found by immunoblotting lower H2AX phosphorylation (γ-H2AX) in post-irradiated $RD^{Cav\text{-}1}$ cells compared to RD^{ctrl} (Fig. 3A), and similar results were also obtained in $RD^{Cav\text{-}1/F1}$ and $RD^{Cav\text{-}1/F2}$ (not shown). We performed a neutral comet assay to quantify the DNA damage. After 1- and 4-hours post-IR, RD^{ctrl} cells showed visibly longer comet tails compared to $RD^{Cav\text{-}1}$ cells, indicative of higher DNA fragmentation (Fig. 3B). By software quantification, we found that irradiated $RD^{Cav\text{-}1}$ cells showed an approximately four-fold reduction in tail DNA fragmentation compared to RD^{ctrl} (Fig. 3B). Since roughly two-thirds of radiation-mediated DNA damage is caused by ROS accumulation [33], we assayed the oxidative stress detection in post-irradiated cells [34]. Five minutes after different IR doses, $RD^{Cav\text{-}1}$ cells showed lower $O_2{\cdot}^-$ levels compared to RD^{ctrl} (Fig. 3C). As reported in supplementary figure 1, we found that IR treatment promoted a strongest antioxidant transcriptional signature in $RD^{Cav\text{-}1}$ cells compared to RD^{ctrl} through the upregulation of antioxidant genes (NRF2, SOD-2, CAT and GPx-4) and miRNAs (miR-22, miR-34a, miR-126, miR-210), as detected by real-time PCR. This suggests that Cav-1 could increase the antioxidant response in post-irradiated cells to prevent abnormal ROS accumulation. We next investigated whether the reduced DNA damage observed in $RD^{Cav\text{-}1}$ cells may be caused by increased repair of damaged DNA. For this purpose, we analyzed by immunoblotting the expression of proteins involved in both homologous recombination (HR) and non-homologous end joining (NHEJ) pathways. Compared to the RD^{ctrl}, we detected in $RD^{Cav\text{-}1}$ cells an increased phosphorylation of ATM, which is needed for DSB repair by HR pathway [35]. In addition, $RD^{Cav\text{-}1}$

cells also showed greater expression of Ku70/80 and phosphorylation of DNA-PK, which are key components of the NHEJ pathway [35] (Fig. 3D). Overall, these data suggest that the reduced DNA damage observed in post-irradiated RD^{Cav-1} cells could be the result of a concomitant increased ability to neutralize ROS species and accelerate DNA repair.

Cav-1 increased GSH content and enhanced protection against H_2O_2 treatment by elevating catalase expression.

Radioresistance is conventionally acquired by tumor cells thanks to elevated antioxidant defense mechanisms, which minimize the effects of IR treatments [36]. We therefore hypothesized that the increased cell survival of RD^{Cav-1} cells might be due to higher expression of antioxidant systems. By using a specific GSH assay, we determined that the intracellular GSH content in RD^{Cav-1} and $RD^{Cav-1/F2}$ cells was approximately of 30 and 22 nmol/mg of protein, respectively, compared to 15 nmol/mg of protein as detected in RD^{ctrl} (Fig. 4A). We next evaluated the total ROS production in cells treated with increasing H_2O_2 doses (from 500 up to 20,000 μM) by using the DCFH-DA probe. Under these conditions, we detected a marked increase of ROS in RD^{ctrl} cells but not in the RD^{Cav-1} and $RD^{Cav-1/F2}$ lines, which maintained low the oxidative stress (Fig. 4B). Due to this unusual resistance to H_2O_2 treatment, we decided to assay the expression of catalase, the enzyme responsible for the H_2O_2 neutralization [37]. We found the enzymatic activity of catalase increased up to 4- and 6-fold in RD^{Cav-1} and $RD^{Cav-1/F2}$ compared to RD^{ctrl}, respectively (Fig. 4C). Consistent with this, immunoblotting showed that the specific protein band of 64 kDa was significantly higher in RD^{Cav-1} and $RD^{Cav-1/F2}$ (Fig. 4D). Taken together, these results indicate that radioresistant RD^{Cav-1} and $RD^{Cav-1/F2}$ cells are characterized by increased catalase expression and GSH content already under basal conditions.

Pharmacological inhibition of Src-kinase and Akt pathways abrogated radioresistance of RD^{Cav-1} cells.

Given the higher content of phosphorylated Cav-1 observed in the radioresistant lines, we hypothesized the activation of Src-kinases, which are known to mediate Cav-1 phosphorylation [38, 39]. In addition, we hypothesized the activation of the serine/threonine kinase Akt, a master regulator of cell survival that activates in response to several genotoxic and damaging agents [40]. By immunoblotting, we found that IR treatment induced pronounced phosphorylation of both Cav-1 and Akt in RD^{Cav-1} cells compared to RD^{ctrl} (Fig. 5A, B). We treated cells with pharmacological inhibitors to evaluate whether the Src-kinase and Akt inhibition could result in diminished radioresistance. By pretreating cells for 2 hours with the Src-kinase inhibitor PP2 or with

the PI3K inhibitor LY294002, we found that the radiosensitivity of RD^{Cav-1} line was restored, as determined by clonogenic assay. In fact, the surviving colony fraction in post-irradiated RD^{Cav-1} cells, respectively treated with PP2 and LY294002, was decreased by approximately 35% and 62% compared to untreated cells (Fig. 5C, D). In addition, we found that these treatments increased IR susceptibility also in RD^{ctrl} cells (Fig. 5C, D). Taken together, these data suggest that Src-kinase and Akt play an important role in radioresistance of RMS.

RD and RH30 lines with acquired radioresistance are characterized by increased expression of Cav-1, Akt and catalase.

By using two recently characterized cell models of ERMS and ARMS radioresistance [28], we evaluated the expression of Cav-1, Akt and catalase. As shown in figure 6A, the radioresistant RD and RH30 lines, named RD^{RR} and $RH30^{RR}$, showed significant increased colony survival after IR compared to parental lines (up to 30% for RD^{RR} and 59% for $RH30^{RR}$). By immunoblotting, we detected that the total and phosphorylated forms of Cav-1 and Akt were significantly increased in RD^{RR} and $RH30^{RR}$ compared to parental lines (Fig. 6B). Furthermore, both radioresistant lines were characterized by the increased basal expression of catalase (Fig. 6B). Finally, we found that radioresistance was significantly inhibited by treatment with PP2 and LY294002 inhibitors (Fig. 6C). Overall, these data confirm that RMS radioresistance is dependent on the concerted activity of Cav-1, Akt and catalase.

Discussion

The data presented here give new insight into the mechanisms of radioresistance in RMS [4], a myogenic tumor that falls into the group of small blue round cell tumors together with neuroblastoma, non-Hodgkin's lymphoma, and the Ewing's family of tumors. Multimodal therapy results in an overall 5-year survival >70% for localized RMS tumors, while metastatic disease has an unfavorable outcome. Radiotherapy is useful in almost all patients with RMS; however, the appearance of resistance mechanisms can promote tumor regrowth and recurrence, leading to treatment failure. This evidence was achieved in a pilot study using ARMS and ERMS lines implanted in xenograft models that developed radiation resistance after fractionated radiotherapy [41]. In 2015, Woods *et al.* [42] also showed a greater propensity for radiotherapy to induce metastasis in some cancer models, including ARMS, suggesting that metastases and recurrent tumors following radiotherapy share underlying molecular mechanisms. In the past decade, our laboratory has documented for the first time the

expression of Cav-1 in RMS tumors [22]. Since in the human RD line, an *in vitro* model of ERMS, Cav-1 is expressed at modest levels, we established engineered cell lines with higher Cav-1 expression, termed RD^{Cav-1}, $RD^{Cav-1/F1}$ and $RD^{Cav-1/F2}$. These lines showed marked tumor aggressiveness and metastatic properties, as observed *in vitro* and *in vivo* [23, 25, 26]. Here we demonstrated that Cav-1 also mediates an increased ability to counteract oxidative stress and repair DNA damage, interfering with cell senescence and apoptosis, and therefore determining a radioresistant cell phenotype. A strong antioxidant signature was associated with Cav-1-mediated radioresistance. In RD^{Cav-1} cells, the radiotherapy promoted a significant transcriptional upregulation of NRF2, SOD-2, CAT and GPx4 genes, which have been widely associated with resistance mechanisms [43]. In this regard, it is important to emphasize that this does not necessarily translates into a net protein increase due to numerous factors. We also found a stronger up-regulation of miR-22 [44], -34a [45], -126 [46], and -210 [47], which have been implicated in cell differentiation of RMS [44], and senescence, inflammation mechanisms and oxidative stress protection in muscle cells [45-47]. Certainly, among the markers indicating the presence of antioxidant signature in RD^{Cav-1} cells, the elevated expression of catalase is particularly intriguing. This homo-tetrameric enzyme (EC 1.11.1.6) is responsible for the decomposition of H_2O_2 [37, 48], and is considered a hallmark of aggressive cancers that develop resistance to chronic exposure to various agents [49], such as cisplatin [50], bleomycin [51], and IR [52]. In addition, catalase overexpression has been shown to protect cells against DNA damage induced by UVB and X-rays [53, 54]. A potential link between Cav-1 and H_2O_2 production has emerged in recent years. In this regard, the loss of Cav-1 has been shown to accentuate the production of H_2O_2, promoting oxidative stress in the tumor microenvironment [55]. Conversely, Cav-1 has been reported to attenuate the production of H_2O_2, negatively affecting the endothelial adhesion of lung cancer cells [56] and limiting DNA damage in lung cancer cells [57]. It is of interest the detection of the highest catalase expression and activity in the more radioresistant $RD^{Cav-1/F2}$ cells, which were derived from lung xenograft noduli and exhibit pronounced metastatic properties [26], suggesting that high catalase expression may represent a hallmark influencing both radioresistance and dissemination processes. It is likely that additional GSH-dependent antioxidant enzymes may be relevant to stress adaptation mechanisms during radioresistance, given the increased amount of GSH found in RD^{Cav-1} cells. GSH has been widely implicated in chemotherapy and radiotherapy resistance of cancer cells [58], and we have recently shown that RD^{Cav-1} cells are vulnerable to oxidative cell death induced by drug depletion of GSH [59]. Enhanced DNA repair is another critical hallmark

recognized in radioresistant cancers. It has been shown that Cav-1 could promote activation of DNA repair pathways [12], as observed in human bronchial carcinoma cell lines [19] and non-small cell lung carcinoma cells [60] by a Cav-1-dependent nuclear translocation of Epidermal growth factor receptor (EGFR) [61, 62]. This mechanism would explain the impaired therapy effectiveness by EGFR antibodies in tumors with nuclear EGFR [63]. In our setting, increased Cav-1 expression associated with stronger activation of the HR and NHEJ pathways, although establish the priority of each pathway in the Cav-1-driven radioresistance requires further work. Interestingly, while Ku70 mediates DNA repair via the NHEJ pathway as part of the Ku70/Ku80 complex [64], Ku70 itself has been reported to inhibit apoptosis [65]. Interestingly, in colon cancer cells Ku70 has been shown to inhibit chemotherapy drug-induced apoptosis by association with Cav-1 [66]. This would suggest that the increased Ku70 levels detected in RD^{Cav-1} cells could be involved in both DNA repair and inhibition of the cell apoptosis. Targeting the activity of Src-kinase and Akt radiosensitized the RD^{Cav-1} cells. The role of these proteins in oxidative stress resistance and DNA repair has been widely documented. Src is aberrantly elevated in may cancers and can activate by receptorial mechanisms [67-69] and increased ROS caused by lipid peroxidation [70]. On the other hand, the serine/threonine Akt kinase is conventionally involved in signaling pathways that inhibit cell apoptosis by increasing protection against oxidative stress [71]. In addition, the Akt1 isoform can also enhance DNA repair in post-irradiated tumor cells by forming a functional complex with the catalytic subunit of DNA-PK [40]. In RMS, Src and Akt are often hyperactivated affecting survival mechanisms [72-74] and drug resistance [75, 76]. Through analysis of RD and RH30 lines that have been repeatedly irradiated to acquire the radioresistance, we obtained confirmation that an adaptative increased expression of Cav-1 and catalase together with the activation of Src-kinase and Akt is critical for radioresistance. Notably, radioresistant lines were characterized by increased Cav-1 phosphorylation, which is known to be mediated by Src-kinase members [38, 39]. Cav-1 phosphorylation, which may increase in response to growth factors [77, 78] and oxidative stress [79-82], activates a variety of intracellular pathways that influence cell morphology [83, 84], migration [85-90], and metastatic properties [8, 9]. Since the Src-inhibition abrogated RMS radioresistance, the hypothesis that Src-kinase through Cav-1 phosphorylation could signal radioresistance mechanisms is fascinating, though requires further investigation. Currently, the development of combined targeted therapies is of great interest to circumvent treatment resistance mechanisms and enhance clinical efficacy in RMS [91]. To our knowledge, while the availability of novel inhibitors of Src-kinase, Akt [92, 93] and DNA damage response pathways [94-96] is

continuously expanding, specific catalase inhibitors are not currently available. In this regard, the effectiveness of tea flavonoids in exhibiting some anticancer properties was related to the ability of the compound epigallocatechin gallate to selectively inhibit catalase [97]. In conclusion, the data reported here suggest that a concerted activity of multiple proteins (Cav-1, catalase) and pathways (HR, NHEJ, Src-kinase, Akt) contributes to oxidative stress protection and DNA repair, and therefore their targeting may represent a promising strategy to overcome radioresistance mechanisms in RMS.

Conflict of interest statement

We have no conflict of interest to declare.

Acknowledgements

This work was supported by an Independent Investigator Grant to AF by Rally Foundation and Infinite Love for Kids Fighting Cancer (20IN19) and by AIRC IG 2020 (ID. 24696) to FM. SC was supported by AIRC fellowship for Italy "Raffaele Anastasio e Lucia Rizzetta in Anastasio" (Rif. 24017). This work is dedicated to the memory of Mia Rose McCaffrey.

Author Contributions

SC, FM, MG, AF planned experiments;

SC, FM, LT, MLB, MG, PC, SG, MA performed experiments;

SC, FM, SMM, VT, PLP, MP, EM and AF analyzed data;

AF wrote the paper.

References

1. Dasgupta R, Fuchs J, Rodeberg D. Rhabdomyosarcoma. Semin Pediatr Surg 2016; 25:276-83.
2. Linardic CM. PAX3-FOXO1 fusion gene in rhabdomyosarcoma. Cancer Lett 2008; 270:10-8.
3. Borinstein SC, Steppan D, Hayashi M, Loeb DM, Isakoff MS, Binitie O, Brohl AS, Bridge JA, Stavas M, Shinohara ET, et al. Consensus and controversies regarding the treatment of rhabdomyosarcoma. Pediatr Blood Cancer 2018; 65.
4. Patel HH, Murray F, Insel PA. Caveolae as organizers of pharmacologically relevant signal transduction molecules. Annu Rev Pharmacol Toxicol 2008; 48:359-91.
5. Parton RG. Caveolae: Structure, Function, and Relationship to Disease. Annu Rev Cell Dev Biol 2018; 34:111-36.

6. Quest AF, Gutierrez-Pajares JL, Torres VA. Caveolin-1: an ambiguous partner in cell signalling and cancer. J Cell Mol Med 2008; 12:1130-50.
7. Goetz JG, Lajoie P, Wiseman SM, Nabi IR. Caveolin-1 in tumor progression: the good, the bad and the ugly. Cancer Metastasis Rev 2008; 27:715-35.
8. Campos A, Burgos-Ravanal R, González MF, Huilcaman R, Lobos González L, Quest AFG. Cell Intrinsic and Extrinsic Mechanisms of Caveolin-1-Enhanced Metastasis. Biomolecules 2019; 9.
9. Wong TH, Dickson FH, Timmins LR, Nabi IR. Tyrosine phosphorylation of tumor cell caveolin-1: impact on cancer progression. Cancer Metastasis Rev 2020.
10. Boscher C, Nabi IR. Caveolin-1: role in cell signaling. Adv Exp Med Biol 2012; 729:29-50.
11. Wang S, Wang N, Zheng Y, Zhang J, Zhang F, Wang Z. Caveolin-1: An Oxidative Stress-Related Target for Cancer Prevention. Oxid Med Cell Longev 2017; 2017:7454031.
12. Zhu H, Yue J, Pan Z, Wu H, Cheng Y, Lu H, Ren X, Yao M, Shen Z, Yang JM. Involvement of Caveolin-1 in repair of DNA damage through both homologous recombination and non-homologous end joining. PLoS One 2010; 5:e12055.
13. Mahmood J, Zaveri SR, Murti SC, Alexander AA, Connors CQ, Shukla HD, Vujaskovic Z. Caveolin-1: a novel prognostic biomarker of radioresistance in cancer. Int J Radiat Biol 2016; 92:747-53.
14. Ketteler J, Klein D. Caveolin-1, cancer and therapy resistance. Int J Cancer 2018.
15. Hehlgans S, Eke I, Storch K, Haase M, Baretton GB, Cordes N. Caveolin-1 mediated radioresistance of 3D grown pancreatic cancer cells. Radiother Oncol 2009; 92:362-70.
16. Duregon E, Senetta R, Pittaro A, Verdun di Cantogno L, Stella G, De Blasi P, Zorzetto M, Mantovani C, Papotti M, Cassoni P. CAVEOLIN-1 expression in brain metastasis from lung cancer predicts worse outcome and radioresistance, irrespective of tumor histotype. Oncotarget 2015; 6:29626-36.
17. Pucci M, Bravatà V, Forte GI, Cammarata FP, Messa C, Gilardi MC, Minafra L. Caveolin-1, breast cancer and ionizing radiation. Cancer Genomics Proteomics 2015; 12:143-52.
18. Barzan D, Maier P, Zeller WJ, Wenz F, Herskind C. Overexpression of caveolin-1 in lymphoblastoid TK6 cells enhances proliferation after irradiation with clinically relevant doses. Strahlenther Onkol 2010; 186:99-106.
19. Dittmann K, Mayer C, Kehlbach R, Rodemann HP. Radiation-induced caveolin-1 associated EGFR internalization is linked with nuclear EGFR transport and activation of DNA-PK. Mol Cancer 2008; 7:69.
20. Rödel F, Capalbo G, Rödel C, Weiss C. Caveolin-1 as a prognostic marker for local control after preoperative chemoradiation therapy in rectal cancer. Int J Radiat Oncol Biol Phys 2009; 73:846-52.
21. Hossain MB, Shifat R, Li J, Luo X, Hess KR, Rivera-Molina Y, Puerta Martinez F, Jiang H, Lang FF, Hung MC, et al. TIE2 Associates with Caveolae and Regulates Caveolin-1 To Promote Their Nuclear Translocation. Mol Cell Biol 2017; 37.
22. Rossi S, Poliani PL, Cominelli M, Bozzato A, Vescovi R, Monti E, Fanzani A. Caveolin 1 is a marker of poor differentiation in Rhabdomyosarcoma. Eur J Cancer 2011; 47:761-72.
23. Faggi F, Mitola S, Sorci G, Riuzzi F, Donato R, Codenotti S, Poliani PL, Cominelli M, Vescovi R, Rossi S, et al. Phosphocaveolin-1 enforces tumor growth and chemoresistance in rhabdomyosarcoma. PLoS One 2014; 9:e84618.
24. Tremblay AM, Missiaglia E, Galli GG, Hettmer S, Urcia R, Carrara M, Judson RN, Thway K, Nadal G, Selfe JL, et al. The Hippo transducer YAP1 transforms activated satellite cells and is a potent effector of embryonal rhabdomyosarcoma formation. Cancer Cell 2014; 26:273-87.
25. Faggi F, Chiarelli N, Colombi M, Mitola S, Ronca R, Madaro L, Bouche M, Poliani PL, Vezzoli M, Longhena F, et al. Cavin-1 and Caveolin-1 are both required to support cell proliferation, migration and anchorage-independent cell growth in rhabdomyosarcoma. Lab Invest 2015.
26. Codenotti S, Faggi F, Ronca R, Chiodelli P, Grillo E, Guescini M, Megiorni F, Marampon F, Fanzani A. Caveolin-1 enhances metastasis formation in a human model of embryonal rhabdomyosarcoma through Erk signaling cooperation. Cancer Lett 2019.
27. Rossi S, Poliani PL, Missale C, Monti E, Fanzani A. Caveolins in rhabdomyosarcoma. J Cell Mol Med 2011; 15:2553-68.

28. Petragnano F, Pietrantoni I, Camero S, Codenotti S, Milazzo L, Vulcano F, Macioce G, Giordani I, Tini P, Cheleschi S, et al. Clinically relevant radioresistant rhabdomyosarcoma cell lines: functional, molecular and immune-related characterization. J Biomed Sci 2020; 27:90.
29. Pawlik TM, Keyomarsi K. Role of cell cycle in mediating sensitivity to radiotherapy. Int J Radiat Oncol Biol Phys 2004; 59:928-42.
30. Smith J, Tho LM, Xu N, Gillespie DA. The ATM-Chk2 and ATR-Chk1 pathways in DNA damage signaling and cancer. Adv Cancer Res 2010; 108:73-112.
31. Petragnano F, Pietrantoni I, Di Nisio V, Fasciani I, Del Fattore A, Capalbo C, Cheleschi S, Tini P, Orelli S, Codenotti S, et al. Modulating the dose-rate differently affects the responsiveness of human epithelial prostate- and mesenchymal rhabdomyosarcoma-cancer cell line to radiation. Int J Radiat Biol 2020:1-13.
32. Kuo LJ, Yang LX. Gamma-H2AX - a novel biomarker for DNA double-strand breaks. In Vivo 2008; 22:305-9.
33. Khanna KK, Jackson SP. DNA double-strand breaks: signaling, repair and the cancer connection. Nat Genet 2001; 27:247-54.
34. Azzam EI, Jay-Gerin JP, Pain D. Ionizing radiation-induced metabolic oxidative stress and prolonged cell injury. Cancer Lett 2012; 327:48-60.
35. Chapman JR, Taylor MR, Boulton SJ. Playing the end game: DNA double-strand break repair pathway choice. Mol Cell 2012; 47:497-510.
36. Sun J, Chen Y, Li M, Ge Z. Role of antioxidant enzymes on ionizing radiation resistance. Free Radic Biol Med 1998; 24:586-93.
37. Nagem RA, Martins EA, Gonçalves VM, Aparício R, Polikarpov I. Crystallization and preliminary X-ray diffraction studies of human catalase. Acta Crystallogr D Biol Crystallogr 1999; 55:1614-5.
38. Glenney JR. Tyrosine phosphorylation of a 22-kDa protein is correlated with transformation by Rous sarcoma virus. J Biol Chem 1989; 264:20163-6.
39. Li S, Seitz R, Lisanti MP. Phosphorylation of caveolin by src tyrosine kinases. The alpha-isoform of caveolin is selectively phosphorylated by v-Src in vivo. J Biol Chem 1996; 271:3863-8.
40. Toulany M, Lee KJ, Fattah KR, Lin YF, Fehrenbacher B, Schaller M, Chen BP, Chen DJ, Rodemann HP. Akt promotes post-irradiation survival of human tumor cells through initiation, progression, and termination of DNA-PKcs-dependent DNA double-strand break repair. Mol Cancer Res 2012; 10:945-57.
41. Kaplon R, Hadziahmetovic M, Sommerfeld J, Bondra K, Lu L, Leasure J, Nguyen P, McHugh K, Li N, Chronowski C, et al. The application of radiation therapy to the Pediatric Preclinical Testing Program (PPTP): results of a pilot study in rhabdomyosarcoma. Pediatr Blood Cancer 2013; 60:377-82.
42. Woods GM, Bondra K, Chronowski C, Leasure J, Singh M, Hensley L, Cripe TP, Chakravarti A, Houghton P. Radiation therapy may increase metastatic potential in alveolar rhabdomyosarcoma. Pediatr Blood Cancer 2015; 62:1550-4.
43. Panieri E, Santoro MM. ROS homeostasis and metabolism: a dangerous liason in cancer cells. Cell Death Dis 2016; 7:e2253.
44. Bersani F, Lingua MF, Morena D, Foglizzo V, Miretti S, Lanzetti L, Carrà G, Morotti A, Ala U, Provero P, et al. Deep Sequencing Reveals a Novel miR-22 Regulatory Network with Therapeutic Potential in Rhabdomyosarcoma. Cancer Res 2016; 76:6095-106.
45. Fulzele S, Mendhe B, Khayrullin A, Johnson M, Kaiser H, Liu Y, Isales CM, Hamrick MW. Muscle-derived miR-34a increases with age in circulating extracellular vesicles and induces senescence of bone marrow stem cells. Aging (Albany NY) 2019; 11:1791-803.
46. Olivieri F, Rippo MR, Monsurrò V, Salvioli S, Capri M, Procopio AD, Franceschi C. MicroRNAs linking inflamm-aging, cellular senescence and cancer. Ageing Res Rev 2013; 12:1056-68.
47. Cicchillitti L, Di Stefano V, Isaia E, Crimaldi L, Fasanaro P, Ambrosino V, Antonini A, Capogrossi MC, Gaetano C, Piaggio G, et al. Hypoxia-inducible factor 1-α induces miR-210 in normoxic differentiating myoblasts. J Biol Chem 2012; 287:44761-71.
48. Gebicka L, Krych-Madej J. The role of catalases in the prevention/promotion of oxidative stress. J Inorg Biochem 2019; 197:110699.
49. Glorieux C, Zamocky M, Sandoval JM, Verrax J, Calderon PB. Regulation of catalase expression in healthy and cancerous cells. Free Radic Biol Med 2015; 87:84-97.

50. Xu H, Choi SM, An CS, Min YD, Kim KC, Kim KJ, Choi CH. Concentration-dependent collateral sensitivity of cisplatin-resistant gastric cancer cell sublines. Biochem Biophys Res Commun 2005; 328:618-22.
51. Yen HC, Li SH, Majima HJ, Huang YH, Chen CP, Liu CC, Tu YC, Chen CW. Up-regulation of antioxidant enzymes and coenzyme Q(10) in a human oral cancer cell line with acquired bleomycin resistance. Free Radic Res 2011; 45:707-16.
52. Lee HC, Kim DW, Jung KY, Park IC, Park MJ, Kim MS, Woo SH, Rhee CH, Yoo H, Lee SH, et al. Increased expression of antioxidant enzymes in radioresistant variant from U251 human glioblastoma cell line. Int J Mol Med 2004; 13:883-7.
53. Epperly MW, Melendez JA, Zhang X, Nie S, Pearce L, Peterson J, Franicola D, Dixon T, Greenberger BA, Komanduri P, et al. Mitochondrial targeting of a catalase transgene product by plasmid liposomes increases radioresistance in vitro and in vivo. Radiat Res 2009; 171:588-95.
54. Rezvani HR, Ged C, Bouadjar B, de Verneuil H, Taïeb A. Catalase overexpression reduces UVB-induced apoptosis in a human xeroderma pigmentosum reconstructed epidermis. Cancer Gene Ther 2008; 15:241-51.
55. Pavlides S, Tsirigos A, Vera I, Flomenberg N, Frank PG, Casimiro MC, Wang C, Fortina P, Addya S, Pestell RG, et al. Loss of stromal caveolin-1 leads to oxidative stress, mimics hypoxia and drives inflammation in the tumor microenvironment, conferring the "reverse Warburg effect": a transcriptional informatics analysis with validation. Cell Cycle 2010; 9:2201-19.
56. Chanvorachote P, Chunhacha P. Caveolin-1 regulates endothelial adhesion of lung cancer cells via reactive oxygen species-dependent mechanism. PLoS One 2013; 8:e57466.
57. Suchaoin W, Chanvorachote P. Caveolin-1 attenuates hydrogen peroxide-induced oxidative damage to lung carcinoma cells. Anticancer Res 2012; 32:483-90.
58. Estrela JM, Ortega A, Obrador E. Glutathione in cancer biology and therapy. Crit Rev Clin Lab Sci 2006; 43:143-81.
59. Codenotti S, Poli M, Asperti M, Zizioli D, Marampon F, Fanzani A. Cell growth potential drives ferroptosis susceptibility in rhabdomyosarcoma and myoblast cell lines. J Cancer Res Clin Oncol 2018; 144:1717-30.
60. Bazzani L, Donnini S, Giachetti A, Christofori G, Ziche M. PGE2 mediates EGFR internalization and nuclear translocation. Oncotarget 2018; 9:14939-58.
61. Lajoie P, Partridge EA, Guay G, Goetz JG, Pawling J, Lagana A, Joshi B, Dennis JW, Nabi IR. Plasma membrane domain organization regulates EGFR signaling in tumor cells. J Cell Biol 2007; 179:341-56.
62. Khan EM, Heidinger JM, Levy M, Lisanti MP, Ravid T, Goldkorn T. Epidermal growth factor receptor exposed to oxidative stress undergoes Src- and caveolin-1-dependent perinuclear trafficking. J Biol Chem 2006; 281:14486-93.
63. Pereira PMR, Sharma SK, Carter LM, Edwards KJ, Pourat J, Ragupathi A, Janjigian YY, Durack JC, Lewis JS. Caveolin-1 mediates cellular distribution of HER2 and affects trastuzumab binding and therapeutic efficacy. Nat Commun 2018; 9:5137.
64. Fell VL, Schild-Poulter C. The Ku heterodimer: function in DNA repair and beyond. Mutat Res Rev Mutat Res 2015; 763:15-29.
65. Kim SH, Kim D, Han JS, Jeong CS, Chung BS, Kang CD, Li GC. Ku autoantigen affects the susceptibility to anticancer drugs. Cancer Res 1999; 59:4012-7.
66. Zou H, Volonte D, Galbiati F. Interaction of caveolin-1 with Ku70 inhibits Bax-mediated apoptosis. PLoS One 2012; 7:e39379.
67. Manning G, Whyte DB, Martinez R, Hunter T, Sudarsanam S. The protein kinase complement of the human genome. Science 2002; 298:1912-34.
68. Roskoski R. Src protein-tyrosine kinase structure, mechanism, and small molecule inhibitors. Pharmacol Res 2015; 94:9-25.
69. Thomas SM, Brugge JS. Cellular functions regulated by Src family kinases. Annu Rev Cell Dev Biol 1997; 13:513-609.
70. Dittmann K, Mayer C, Kehlbach R, Rothmund MC, Peter Rodemann H. Radiation-induced lipid peroxidation activates src kinase and triggers nuclear EGFR transport. Radiother Oncol 2009; 92:379-82.

71. Wang X, McCullough KD, Franke TF, Holbrook NJ. Epidermal growth factor receptor-dependent Akt activation by oxidative stress enhances cell survival. J Biol Chem 2000; 275:14624-31.
72. Petricoin EF, Espina V, Araujo RP, Midura B, Yeung C, Wan X, Eichler GS, Johann DJ, Qualman S, Tsokos M, et al. Phosphoprotein pathway mapping: Akt/mammalian target of rapamycin activation is negatively associated with childhood rhabdomyosarcoma survival. Cancer Res 2007; 67:3431-40.
73. Shern JF, Chen L, Chmielecki J, Wei JS, Patidar R, Rosenberg M, Ambrogio L, Auclair D, Wang J, Song YK, et al. Comprehensive genomic analysis of rhabdomyosarcoma reveals a landscape of alterations affecting a common genetic axis in fusion-positive and fusion-negative tumors. Cancer Discov 2014; 4:216-31.
74. Seki M, Nishimura R, Yoshida K, Shimamura T, Shiraishi Y, Sato Y, Kato M, Chiba K, Tanaka H, Hoshino N, et al. Integrated genetic and epigenetic analysis defines novel molecular subgroups in rhabdomyosarcoma. Nat Commun 2015; 6:7557.
75. Yeung CL, Ngo VN, Grohar PJ, Arnaldez FI, Asante A, Wan X, Khan J, Hewitt SM, Khanna C, Staudt LM, et al. Loss-of-function screen in rhabdomyosarcoma identifies CRKL-YES as a critical signal for tumor growth. Oncogene 2013; 32:5429-38.
76. Casini N, Forte IM, Mastrogiovanni G, Pentimalli F, Angelucci A, Festuccia C, Tomei V, Ceccherini E, Di Marzo D, Schenone S, et al. SRC family kinase (SFK) inhibition reduces rhabdomyosarcoma cell growth in vitro and in vivo and triggers p38 MAP kinase-mediated differentiation. Oncotarget 2015; 6:12421-35.
77. Fielding PE, Chau P, Liu D, Spencer TA, Fielding CJ. Mechanism of platelet-derived growth factor-dependent caveolin-1 phosphorylation: relationship to sterol binding and the role of serine-80. Biochemistry 2004; 43:2578-86.
78. Orlichenko L, Huang B, Krueger E, McNiven MA. Epithelial growth factor-induced phosphorylation of caveolin 1 at tyrosine 14 stimulates caveolae formation in epithelial cells. J Biol Chem 2006; 281:4570-9.
79. Volonté D, Galbiati F, Pestell RG, Lisanti MP. Cellular stress induces the tyrosine phosphorylation of caveolin-1 (Tyr(14)) via activation of p38 mitogen-activated protein kinase and c-Src kinase. Evidence for caveolae, the actin cytoskeleton, and focal adhesions as mechanical sensors of osmotic stress. J Biol Chem 2001; 276:8094-103.
80. Sanguinetti AR, Mastick CC. c-Abl is required for oxidative stress-induced phosphorylation of caveolin-1 on tyrosine 14. Cell Signal 2003; 15:289-98.
81. Sanguinetti AR, Cao H, Corley Mastick C. Fyn is required for oxidative- and hyperosmotic-stress-induced tyrosine phosphorylation of caveolin-1. Biochem J 2003; 376:159-68.
82. Wehinger S, Ortiz R, Díaz MI, Aguirre A, Valenzuela M, Llanos P, Mc Master C, Leyton L, Quest AF. Phosphorylation of caveolin-1 on tyrosine-14 induced by ROS enhances palmitate-induced death of beta-pancreatic cells. Biochim Biophys Acta 2015; 1852:693-708.
83. Joshi B, Bastiani M, Strugnell SS, Boscher C, Parton RG, Nabi IR. Phosphocaveolin-1 is a mechanotransducer that induces caveola biogenesis via Egr1 transcriptional regulation. J Cell Biol 2012; 199:425-35.
84. Zimnicka AM, Husain YS, Shajahan AN, Sverdlov M, Chaga O, Chen Z, Toth PT, Klomp J, Karginov AV, Tiruppathi C, et al. Src-dependent phosphorylation of caveolin-1 Tyr-14 promotes swelling and release of caveolae. Mol Biol Cell 2016; 27:2090-106.
85. Gottlieb-Abraham E, Shvartsman DE, Donaldson JC, Ehrlich M, Gutman O, Martin GS, Henis YI. Src-mediated caveolin-1 phosphorylation affects the targeting of active Src to specific membrane sites. Mol Biol Cell 2013; 24:3881-95.
86. Joshi B, Strugnell SS, Goetz JG, Kojic LD, Cox ME, Griffith OL, Chan SK, Jones SJ, Leung SP, Masoudi H, et al. Phosphorylated caveolin-1 regulates Rho/ROCK-dependent focal adhesion dynamics and tumor cell migration and invasion. Cancer Res 2008; 68:8210-20.
87. Meng F, Saxena S, Liu Y, Joshi B, Wong TH, Shankar J, Foster LJ, Bernatchez P, Nabi IR. The phospho-caveolin-1 scaffolding domain dampens force fluctuations in focal adhesions and promotes cancer cell migration. Mol Biol Cell 2017; 28:2190-201.
88. Grande-García A, Echarri A, de Rooij J, Alderson NB, Waterman-Storer CM, Valdivielso JM, del Pozo MA. Caveolin-1 regulates cell polarization and directional migration through Src kinase and Rho GTPases. J Cell Biol 2007; 177:683-94.

89. Goetz JG, Joshi B, Lajoie P, Strugnell SS, Scudamore T, Kojic LD, Nabi IR. Concerted regulation of focal adhesion dynamics by galectin-3 and tyrosine-phosphorylated caveolin-1. J Cell Biol 2008; 180:1261-75.
90. Urra H, Torres VA, Ortiz RJ, Lobos L, Díaz MI, Díaz N, Härtel S, Leyton L, Quest AF. Caveolin-1-enhanced motility and focal adhesion turnover require tyrosine-14 but not accumulation to the rear in metastatic cancer cells. PLoS One 2012; 7:e33085.
91. van Erp AEM, Versleijen-Jonkers YMH, van der Graaf WTA, Fleuren EDG. Targeted Therapy-based Combination Treatment in Rhabdomyosarcoma. Mol Cancer Ther 2018; 17:1365-80.
92. Guenther MK, Graab U, Fulda S. Synthetic lethal interaction between PI3K/Akt/mTOR and Ras/MEK/ERK pathway inhibition in rhabdomyosarcoma. Cancer Lett 2013; 337:200-9.
93. Renshaw J, Taylor KR, Bishop R, Valenti M, De Haven Brandon A, Gowan S, Eccles SA, Ruddle RR, Johnson LD, Raynaud FI, et al. Dual Blockade of the PI3K/AKT/mTOR (AZD8055) and RAS/MEK/ERK (AZD6244) Pathways Synergistically Inhibits Rhabdomyosarcoma Cell Growth In Vitro and In Vivo. Clin Cancer Res 2013; 19:5940-51.
94. Fam HK, Walton C, Mitra SA, Chowdhury M, Osborne N, Choi K, Sun G, Wong PC, O'Sullivan MJ, Turashvili G, et al. TDP1 and PARP1 deficiency are cytotoxic to rhabdomyosarcoma cells. Mol Cancer Res 2013; 11:1179-92.
95. Norris RE, Adamson PC, Nguyen VT, Fox E. Preclinical evaluation of the PARP inhibitor, olaparib, in combination with cytotoxic chemotherapy in pediatric solid tumors. Pediatr Blood Cancer 2014; 61:145-50.
96. Smith MA, Reynolds CP, Kang MH, Kolb EA, Gorlick R, Carol H, Lock RB, Keir ST, Maris JM, Billups CA, et al. Synergistic activity of PARP inhibition by talazoparib (BMN 673) with temozolomide in pediatric cancer models in the pediatric preclinical testing program. Clin Cancer Res 2015; 21:819-32.
97. Pal S, Dey SK, Saha C. Inhibition of catalase by tea catechins in free and cellular state: a biophysical approach. PLoS One 2014; 9:e102460.

Author Contributions

SC, FM, MG, AF planned experiments;

SC, FM, LT, MLB, MG, PC, SG, MA performed experiments;

SC, FM, SMM, VT, PLP, MP, EM and AF analyzed data;

AF wrote the paper.

Figure legends

Figure 1. Analysis of cell survival in post-irradiated cells. A) Immunoblotting detection of Cav-1, total and Tyr-14-phosphorylated (pCav-1) forms, in RD^{ctrl}, RD^{Cav-1}, $RD^{Cav-1/F1}$, and $RD^{Cav-1/F2}$ lines. Total protein homogenates were prepared after 48 hours of cell growth. Tubulin served as loading control and protein quantification is expressed by arbitrary density units (n=4). Data are Mean ± SEM, *** p-value<0.0001; One-Way Anova test. B) Clonogenic evaluation of cell survival in lines treated with increasing IR doses. The images show surviving cell colonies after crystal violet staining. The graph represents the fraction of the surviving cell colonies after the colorimetric quantification of the crystal violet (n=2). Data are Mean ± SEM, ** p-value<0.001; *** p-value<0.0001; One-Way Anova test.

Figure 2. Analysis of cell cycle, apoptosis and senescence markers in post-irradiated cells. A) Immunoblotting detection of Chk1 or Chk2, total and phosphorylated forms (pChk1 and pChk2), on post-irradiated control and RD^{Cav-1} lines at the indicated time points. Tubulin served as loading control and protein quantification is expressed by arbitrary density units (n=4). Data are Mean ± SEM, ** p-value<0.001; *** p-value<0.0001; One-Way Anova test. B) FACS analysis performed 24 hours after IR on control and RD^{Cav-1} lines. The pie charts show the percentage of cells in the G1, S and G2 phases of the cell cycle (n=3). C-F) Control and RD^{Cav-1} lines were given two consecutive IR doses (4 Gy each) 24 hours apart. C,D) The histogram report the percentage of apoptotic cells (C) and senescent cells (D), detected after 1, 3, and 6 days from the second IR treatment by TUNEL test and β-galactosidase test, respectively (n=3). Data are Mean ± SEM, ** p-value<0.001; *** p-value<0.0001; Unpaired Student's t-test. E, F) Immunoblotting detection of the cleaved Caspase-3 (E) and $p21^{Cip1/Waf1}$ and $p16^{INK4a}$ (F) 24 hours after the second IR treatment. Tubulin served as loading control and protein quantification is expressed by arbitrary density units (n=3). Data are Mean ± SEM, ** p-value<0.001; *** p-value<0.0001; Unpaired Student's t-test.

Figure 3. Analysis of DNA damage, ROS levels and DNA repair proteins in post-irradiated cells. Control and RD^{Cav-1} lines were given IR treatment (4 Gy). A) Immunoblotting detection of ɣ-H2AX in post-irradiated cells at the indicated time points. Tubulin served as loading control and protein quantification is expressed by arbitrary density units (n=3). Data are Mean ± SEM, * p-value<0.05; ** p-value<0.001; *** p-value<0.0001; One-Way Anova test. B) DNA fragmentation was evaluated 1 and 4 hours after IR by the comet assay. The pictures were taken at 10x magnification. The graph represents the percentage of fragmented DNA in the comet

tail after quantification (n=3). Data are Mean ± SEM, ** p-value<0.001; *** p-value<0.0001 vs untreated cells; One-Way Anova test. # p-value<0.05; # # # p-value<0.0001 vs RD^{ctrl} cells; Unpaired Student's t-test. C) Control and RD^{Cav-1} lines were given increasing IR doses. After 5 minutes, the $O_2 \cdot^-$ production was detected (n=3). Data are Mean ± SEM, * p-value<0.05; ** p-value<0.001; Unpaired Student's t-test. D) Immunoblotting detection of total and phosphorylated ATM form (pATM), Ku70, Ku80, and total and phosphorylated DNA-PK form (pDNA-PK) in post-irradiated cells at the indicated time points. Tubulin served as loading control and protein quantification is expressed by arbitrary density units (n=3). Data are Mean ± SEM, * p-value<0.05; ** p-value<0.001; *** p-value<0.0001; One-Way Anova test.

Figure 4. Analysis of antioxidant scavenger systems. A) The amount of GSH content was quantified in the different lines (n=3). Data are Mean ± SEM, ** p-value<0.001; *** p-value<0.0001; One-Way Anova test. B) The fluorogenic probe DCFH-DA was administered to quantify the total ROS production in control, RD^{Cav-1} and $RD^{Cav-1/F2}$ cells treated or not with increasing H_2O_2 doses (n=3). Data are Mean ± SEM, *** p-value<0.0001; One-Way Anova test. C) The enzymatic activity of catalase was assayed in the lines after 48 hours of cell growth. (n=3). Data are Mean ± SEM, * p-value<0.05; *** p-value<0.0001; One-Way Anova test. D) Immunoblotting detection of catalase in the different cell lines. Tubulin served as loading control and protein quantification is expressed by arbitrary density units (n=3). Data are Mean ± SEM, *** p-value<0.0001; One-Way Anova test.

Figure 5. Analysis of Cav-1 and Akt phosphorylation in post-irradiated cells. A, B**)** Immunoblotting detection of Cav-1 (total and pCav-1) (A) and Akt (total and pAkt) (B) in post-irradiated control and RD^{Cav-1} lines at the indicated time points. Tubulin served as loading control and protein quantification is expressed by arbitrary density units (n=3). Data are Mean ± SEM, * p-value<0.05; *** p-value<0.0001; One-Way Anova test. C, D) Clonogenic evaluation of cell survival in post-irradiated control and RD^{Cav-1} cells pre-treated or not with PP2 (C) or LY294002 (D) compared to DMSO. The images show surviving cell colonies after crystal violet staining. The graph represents the fraction of the surviving cell colonies after the colorimetric quantification of the crystal violet (n=3). Data are Mean ± SEM, * p-value<0.05; *** p-value<0.0001; Unpaired Student's t-test.

Figure 6. Analysis of radioresistant RD^{RR} and $RH30^{RR}$ lines. A) Clonogenic evaluation of cell survival in post-irradiated radioresistant and parental lines. The images show surviving cell colonies after crystal violet

staining. The graph represents the fraction of the surviving cell colonies after the colorimetric quantification of the crystal violet (n=2). Data are Mean ± SEM, *** p-value<0.0001; Unpaired Student's t-test. B) Immunoblotting detection of Cav-1 (total and pCav-1), Akt (total and pAkt) and catalase in radioresistant and parental lines. Cells were collected after 48 hours of cell growth. Tubulin served as loading control and protein quantification is expressed by arbitrary density units (n=4). Data are Mean ± SEM, ** p-value<0.001; *** p-value<0.0001; Unpaired Student's t-test. C) Clonogenic evaluation of cell survival in post-irradiated RD^{RR} and $RH30^{RR}$ lines, pretreated for 2 hours with either PP2 or LY294002 compared to DMSO-treated cells. The images show surviving cell colonies after crystal violet staining. The graph represents the fraction of the surviving cell colonies after the colorimetric quantification of the crystal violet (n=3). Data are Mean ± SEM, ** p-value<0.001; *** p-value<0.0001; One-Way Anova test.

Figure S1. Real-time PCR analysis on post-irradiated control and $RD^{Cav\text{-}1}$ lines. The expression of antioxidant genes (A-D) and miRNAs (E-H) was evaluated in cells 12 hours after IR treatment (n=3). Data are Mean ± SEM, * p-value<0.05; ** p-value<0.001; *** p-value<0.0001 vs untreated cells; Unpaired Student's t-test. # # # p-value<0.0001 vs RD^{ctrl} cells; Unpaired Student's t-test.

Figure 1

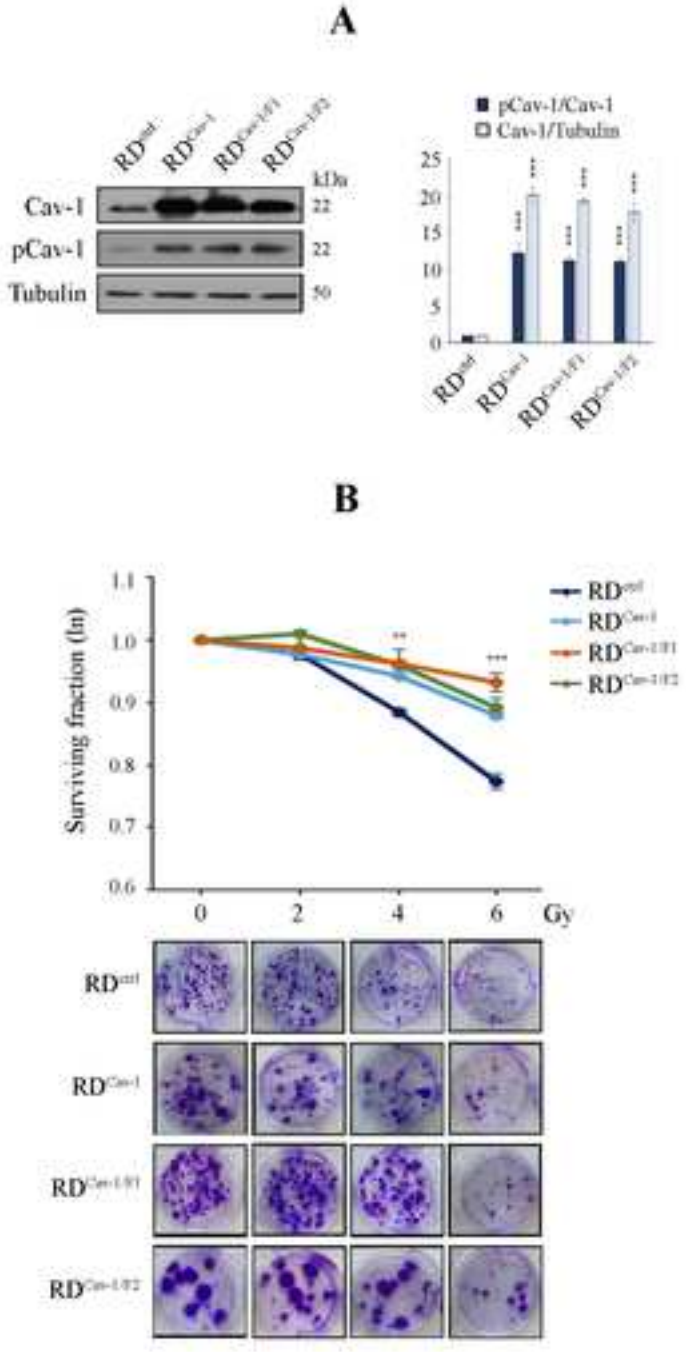

Figure 2

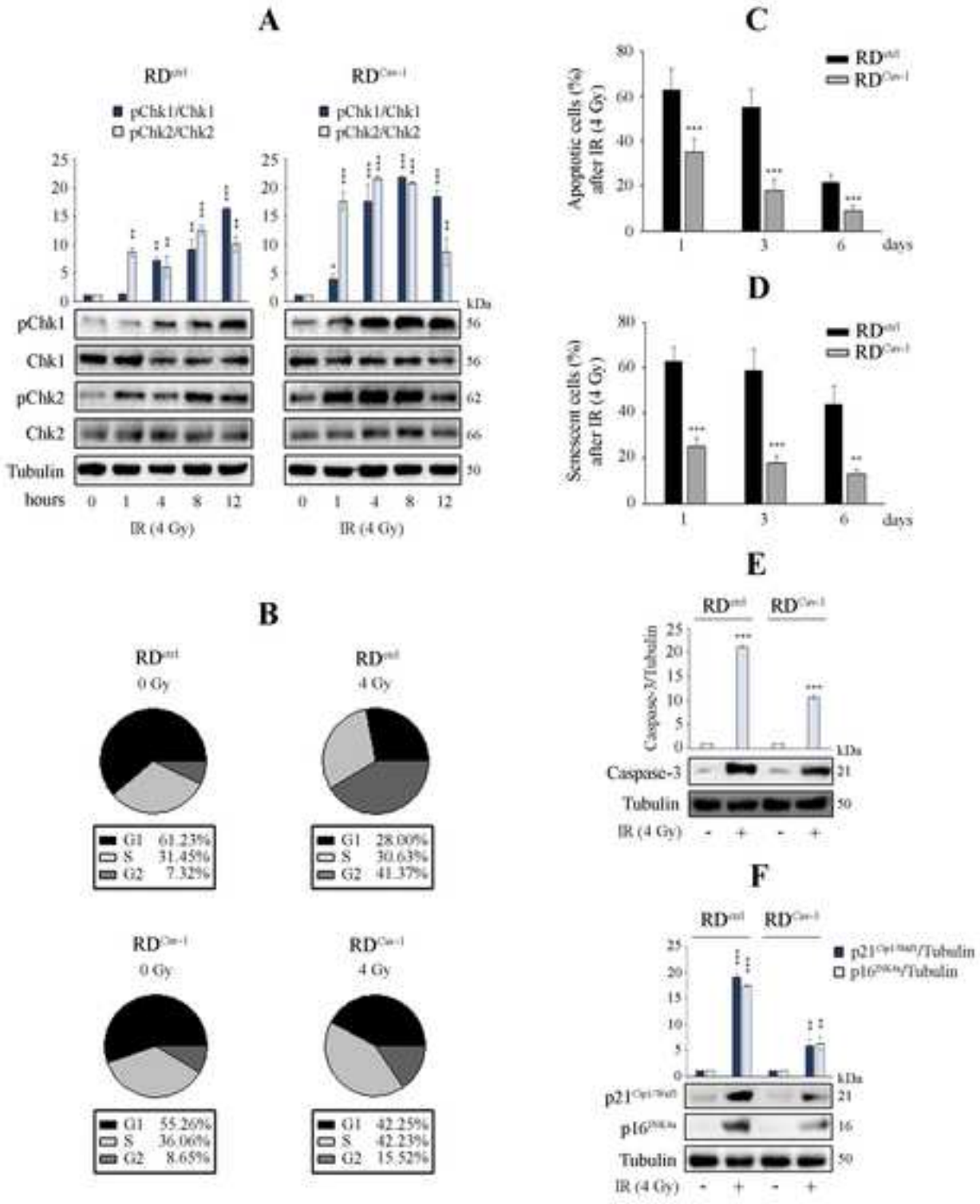
A
RD
RD
pChk1/Chk1
pChk2/Chk2
pChk1/Chk1
pChk2/Chk2
kDa
pChk1
Chk1
pChk2
Chk2
Tubulin
hours 0 1 4 8 12
IR (4 Gy)
IR (4 Gy)
B
RD 0 Gy
RD 4 Gy
G1 61.23%
S 31.45%
G2 7.32%
G1 28.00%
S 30.63%
G2 41.37%
RD 0 Gy
RD 4 Gy
G1 55.26%
S 36.06%
G2 8.65%
G1 42.25%
S 42.23%
G2 15.52%
C
Apoptotic cells (%) after IR (4 Gy)
days
D
Senescent cells (%) after IR (4 Gy)
days
E
Caspase-3/Tubulin
Caspase-3
Tubulin
IR (4 Gy)
F
p21/Tubulin
p16/Tubulin
p21
p16
Tubulin
IR (4 Gy)

Figure 3

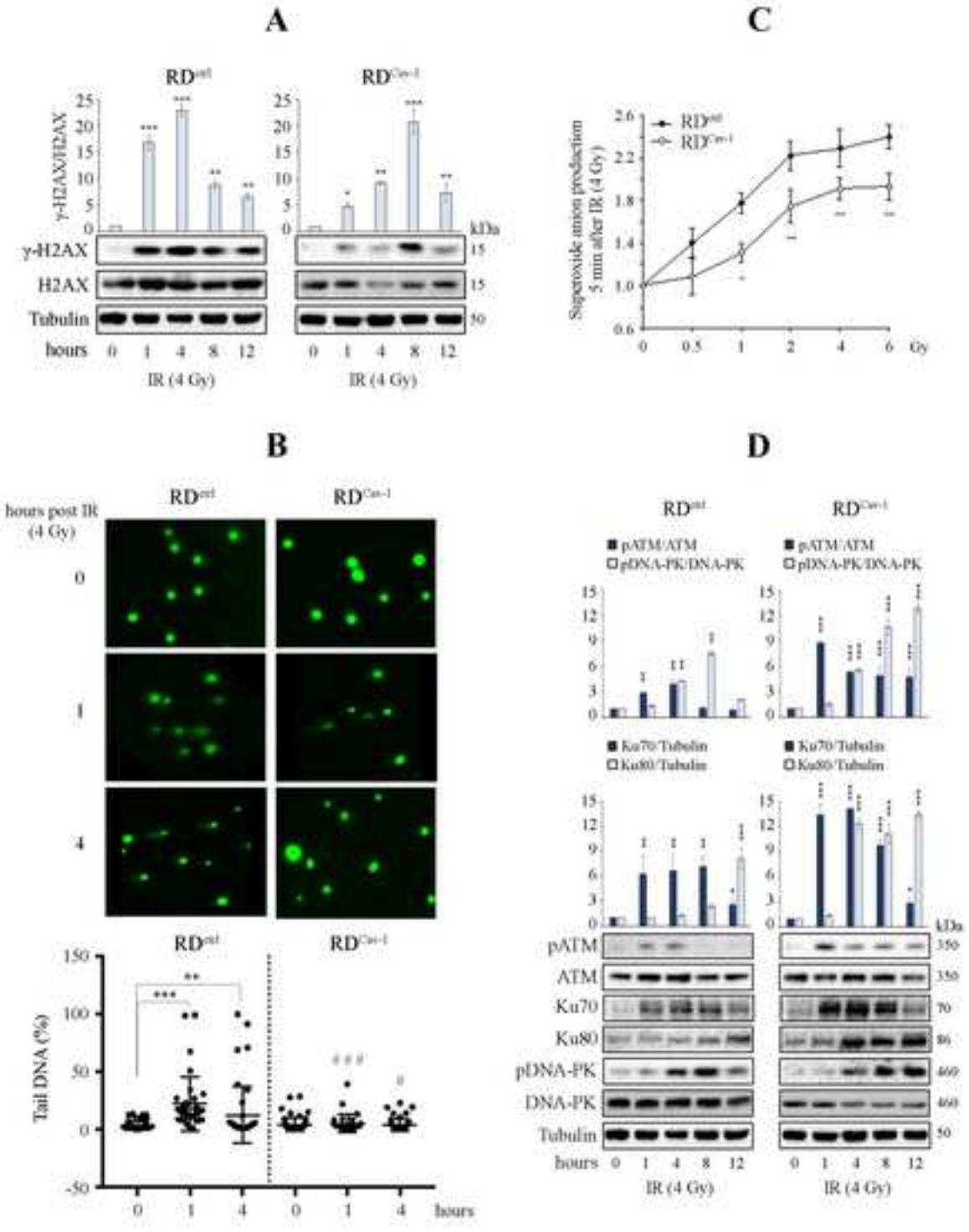
A
C
B
D
γ-H2AX/H2AX
γ-H2AX
H2AX
Tubulin
hours
IR (4 Gy)
kDa
Superoxide anion production 5 min after IR (4 Gy)
Gy
hours post IR (4 Gy)
Tail DNA (%)
pATM/ATM
pDNA-PK/DNA-PK
Ku70/Tubulin
Ku80/Tubulin
pATM
ATM
Ku70
Ku80
pDNA-PK
DNA-PK
Tubulin

Figure 4

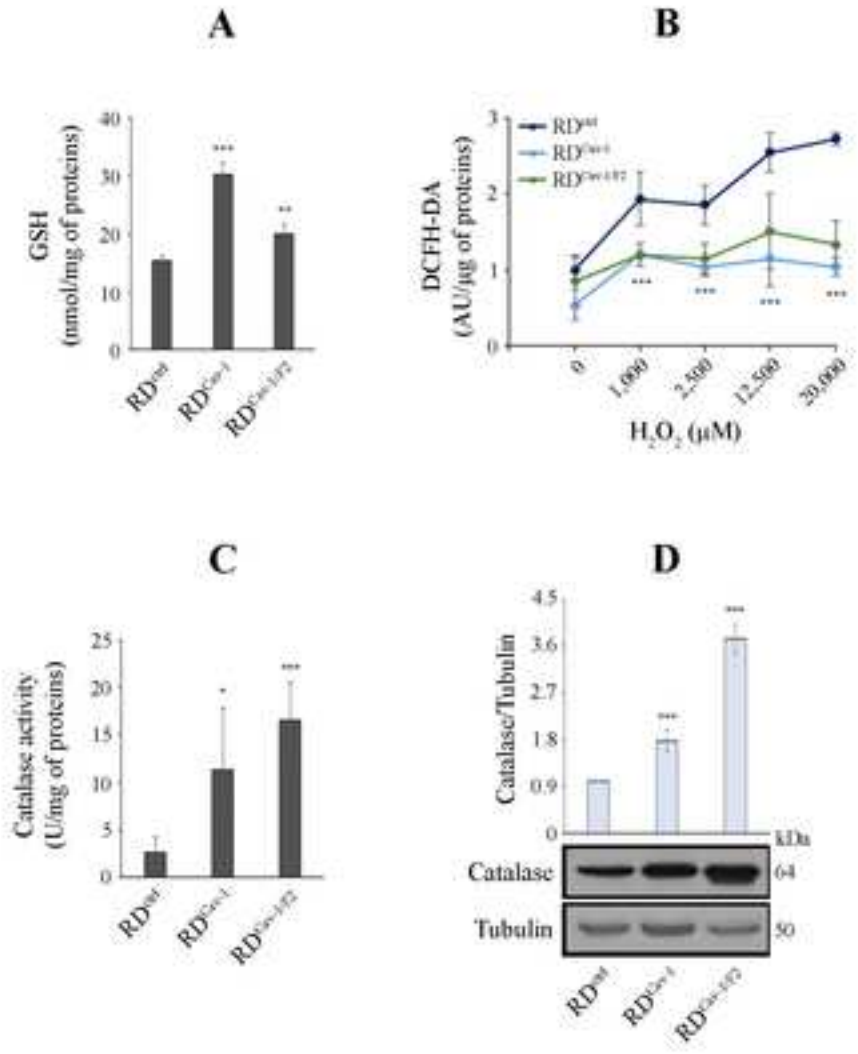

Figure 5

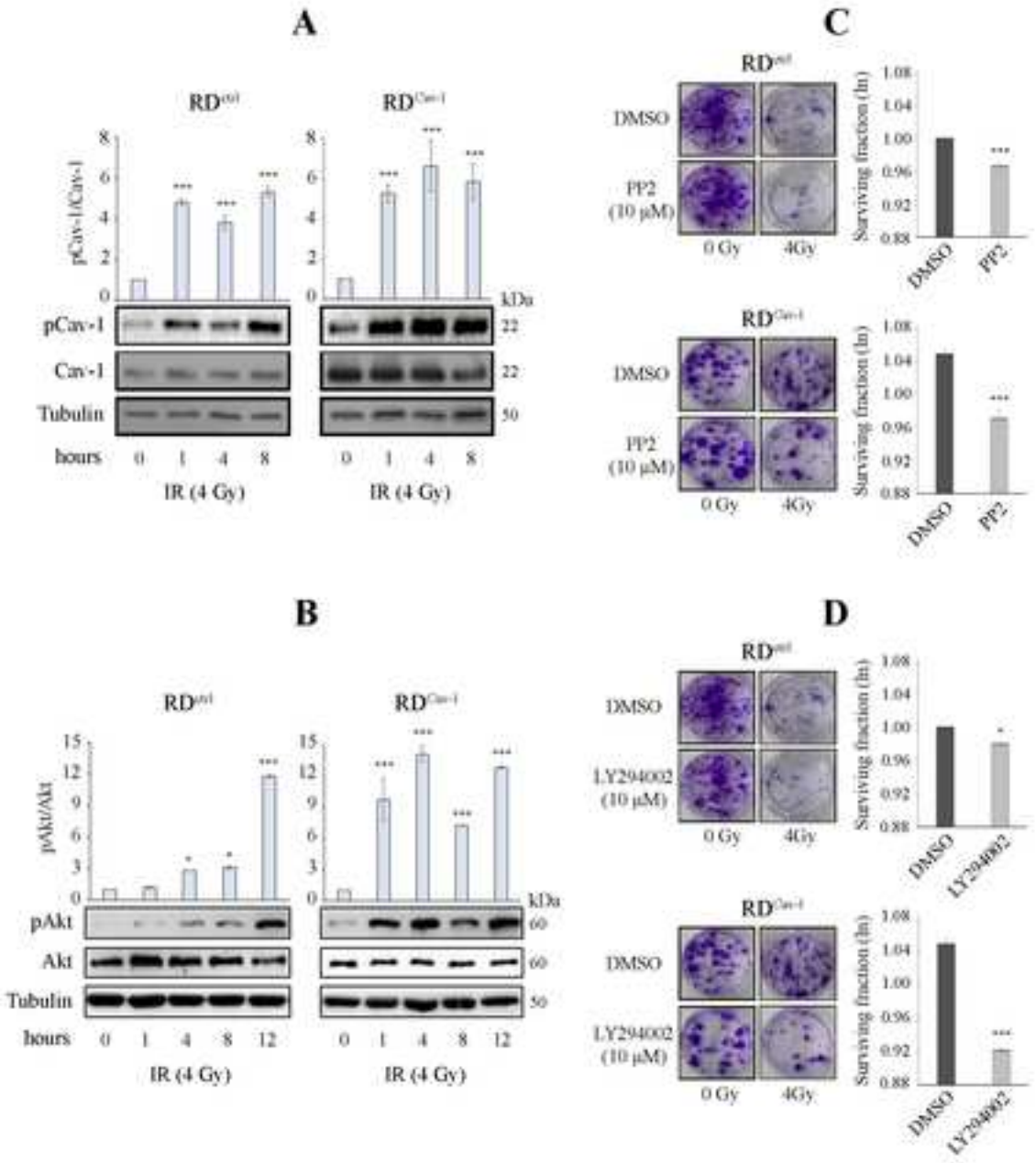

Figure 6

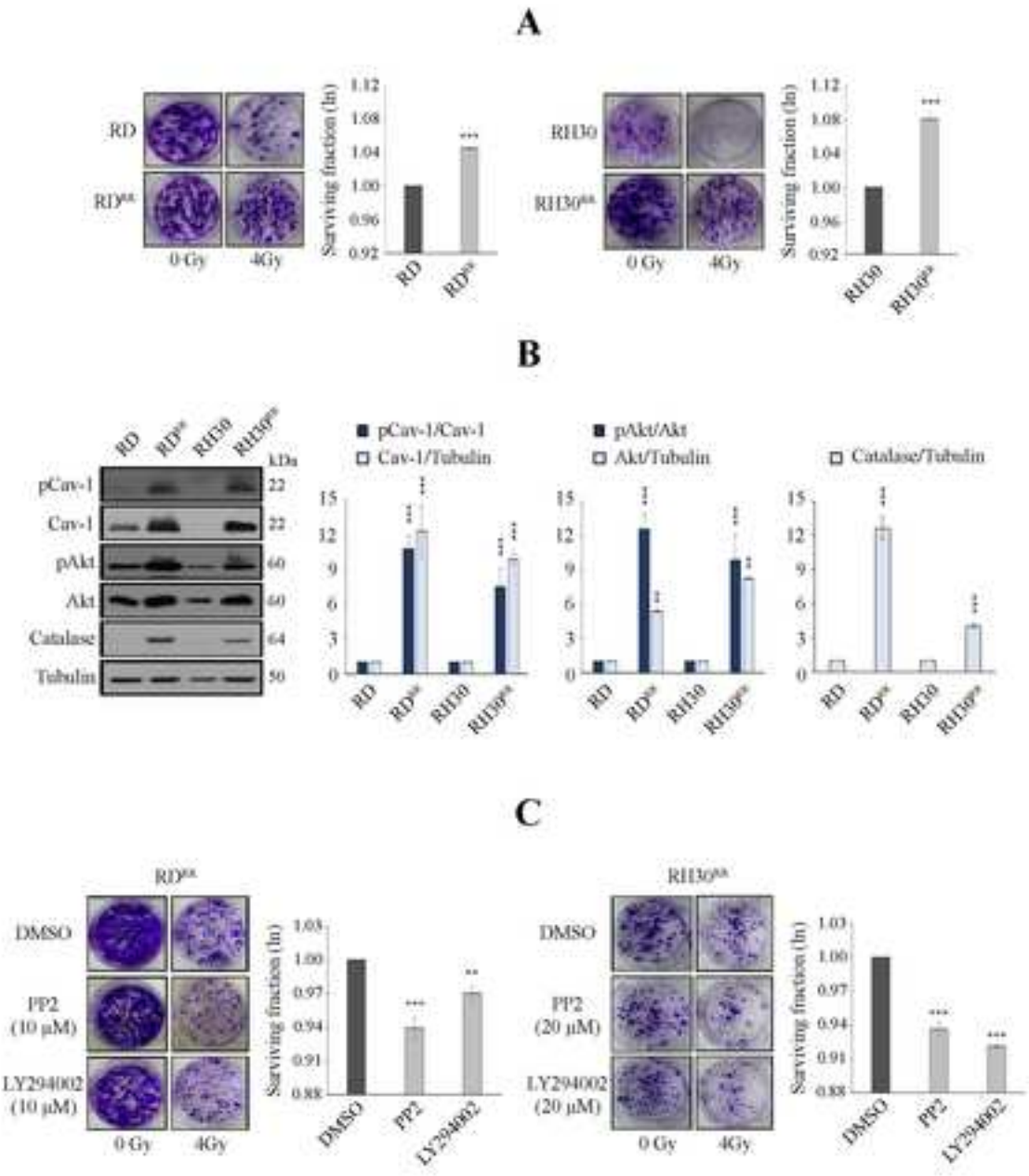
A
RD
RD^RR
0 Gy
4Gy
Surviving fraction (ln)
1.12
1.08
1.04
1.00
0.96
0.92
***
RD
RD^RR
RH30
RH30^RR
RH30
RH30^RR
B
RD
RD^RR
RH30
RH30^RR
kDa
pCav-1
Cav-1
pAkt
Akt
Catalase
Tubulin
22
22
60
60
64
50
pCav-1/Cav-1
Cav-1/Tubulin
pAkt/Akt
Akt/Tubulin
Catalase/Tubulin
15
12
9
6
3
0
C
RD^RR
RH30^RR
DMSO
PP2
(10 μM)
LY294002
(10 μM)
PP2
(20 μM)
LY294002
(20 μM)
0 Gy
4Gy
Surviving fraction (ln)
1.03
1.00
0.97
0.94
0.91
0.88
***
**
DMSO
PP2
LY294002